Available online at www.sciencedirect.com

SciVerse ScienceDirect

Physics Procedia 28 (2012) 72 – 78

Physics Procedia

Electronic band structure of polytypical nanowhiskers

Paulo Eduardo de Faria Junior[a,1], Guilherme Matos Sipahi[a]

[a] *Universidade de São Paulo, Instituto de Física de São Carlos, São Carlos-SP 13560-970, Brazil*

Abstract

III-V compound nanowhiskers have attracted much attention recently due to their distinguished electronic and optical properties. In these nanostructures it was observed a phenomenon called polytypism, i. e., a phase alternation between zinc-blend and wurtzite structure. Although the polytypical effect is now well controlled, a more detailed band structure model is not still done, especially in the vicinity of the band edges. In this theoretical study we propose a model to calculate the electronic band structure in the vicinity of the band edges for polytypical nanowhiskers. Relying on group theory concepts and on the k·p method we connected the irreducible representations at the Γ-point of the two crystal structures and described them in a single matrix. Our results for InP show the carriers' spatial separation which agrees with reported experiments.

Keywords: polytypism, nanowhiskers, band structure, k·p method, group theory

1. Introduction

An increasing number of papers have reported high quality and control growth for nanowires and nanowhiskers (NWs) of III-V compounds including InP, InAs, GaAs and GaP [1, 2, 3, 4, 5, 6, 7]. Nanoelectronics, nanophotonics and solar cells are some of the possible technological applications of these nanostructures.

Although most of the III-V compounds (phosphides, arsenides and antimonides) have zinc-blend (ZB) as the most stable phase, reducing the dimensions to the nanoscale level can change the crystal structure to the wurtzite (WZ) phase. The natural explanation to this behavior is the small formation energy difference between the two crystal structures. In fact, both ZB and WZ structures are very similar when looking through the [111] ZB or [0001] WZ growth directions and can be described as stacked hexagonal layers. An extensive summary of NWs growth, properties and applications was made by Dubrovskii *et al.* [8].

From the theoretical point of view, there are very few papers regarding band structure calculations [9, 10]. A theoretical model for this new kind of nanostructures can lead to band gap engineering and novel electronic properties and also serve as a guide for the crystal growth community.

We developed a model to calculate the electronic properties of polytypical NWs using the schematics provided by Murayama and Nakayama [11] to relate the states of the WZ and ZB structures at the interface based on their symmetry and the k·p method.

[1] Corresponding Author, Tel.: +55-16-3373-9856
Email Address: fariajunior.pe@gmail.com

1875-3892 doi:10.1016/j.phpro.2012.03.674

2. Theoretical Model

In our model [12] we used group theory concepts to relate the irreducible representations in the WZ/ZB interface of the polytypic NWs, and the k·p method to construct the dispersion relations for the desired energy bands. In this paper, we will consider only the lowest conduction band and the top three valence bands.

The connection of the irreducible representations can be obtained using the relations presented in [11, 13]. Through those relations we could select the energy bands connected by symmetry and consequently determine the matrix elements of the Hamiltonian.

In polytypical nanowhiskers, the growth of the ZB phase is oriented along [111] direction implying that the representation must be done in this particular direction. Then, we have two different choices in the description: to calculate all the symmetry operations in the [111] coordinate system (which is the same as the [0001] WZ direction) in order to obtain the matrix elements or to apply a basis rotation to the ZB [001] k·p matrix.

Considering the rotation of axes as reported by [14] and dropping out the prime of the notation, the $\{|c_l\rangle\}$ basis for both crystal structures is defined as:

$$\begin{aligned}
|c_1\rangle &= -\frac{1}{\sqrt{2}}\,|(X+iY)\uparrow\rangle \\
|c_2\rangle &= \frac{1}{\sqrt{2}}\,|(X-iY)\uparrow\rangle \\
|c_3\rangle &= |Z\uparrow\rangle \\
|c_4\rangle &= \frac{1}{\sqrt{2}}\,|(X-iY)\downarrow\rangle \\
|c_5\rangle &= -\frac{1}{\sqrt{2}}\,|(X+iY)\downarrow\rangle \\
|c_6\rangle &= |Z\downarrow\rangle \\
|c_7\rangle &= i\,|S\uparrow\rangle \\
|c_8\rangle &= i\,|S\downarrow\rangle
\end{aligned} \tag{1}$$

For simplicity, the interband interaction is not taken into account here thus the conduction band is a single band model for spin-up and spin-down reading as

$$E_C(\vec{k}) = E_g + E_{OFF} + \frac{\hbar^2}{2m_e^{\parallel}}k_z^2 + \frac{\hbar^2}{2m_e^{\perp}}\left(k_x^2 + k_y^2\right) \tag{2}$$

where E_g is the gap energy, E_{OFF} is used if the valence band maximum is not set to zero and $m_e^{\parallel}$, $m_e^{\perp}$ are the electron effective masses parallel and perpendicular do the z axis, respectively. For the ZB structure, $m_e^{\parallel} = m_e^{\perp}$.

The Hamiltonian for the valence band of the two crystal structures is

$$H_V = \begin{bmatrix}
F & -K^* & -H^* & 0 & 0 & 0 \\
-K & G & H & 0 & 0 & \Delta \\
-H & H^* & \lambda & 0 & \Delta & 0 \\
0 & 0 & 0 & F & -K & H \\
0 & 0 & \Delta & -K^* & G & -H^* \\
0 & \Delta & 0 & H^* & -H & \lambda
\end{bmatrix} \tag{3}$$

the matrix terms being defined as

$$\begin{aligned}
F &= \Delta_1 + \Delta_2 + \lambda + \theta \\
G &= \Delta_1 - \Delta_2 + \lambda + \theta \\
\lambda &= A_1 k_z^2 + A_2\left(k_x^2 + k_y^2\right) \\
\theta &= A_3 k_z^2 + A_4\left(k_x^2 + k_y^2\right)
\end{aligned}$$

$$\begin{aligned} K &= A_5 k_+^2 + 2\sqrt{2} A_z k_- k_z \\ H &= A_6 k_+ k_z + A_z k_-^2 \\ \Delta &= \sqrt{2}\Delta_3 \end{aligned} \tag{4}$$

where $k_\pm = k_x \pm i k_y$, $A_i (i = 1, ..., 6, z)$ are the effective mass parameters, Δ_1 is the crystal field splitting energy and $\Delta_{2,3}$ are the spin-orbit splitting energies.

It is important to notice that the parameter A_z was introduced to provide the correct description of the ZB band structure, retrieving its correct symmetry description. In the regions where the crystal structure is WZ, this parameter is set to zero. As a consequence of the procedure described above, the WZ $A_i (i = 1, ..., 6)$ parameters together with the new parameter A_z are related to the $\gamma_i (i = 1, 2, 3)$ ZB parameters. Also, $\Delta_{2,3}$ WZ parameters are related to Δ_{SO} and Δ_1 is zero for the ZB region.

To evaluate the correctness and reliability of our description, we applied our method to calculate the valence band of bulk WZ and ZB InP. Figure 1 presents the valence band structure calculated for both phases. The ZB parameters were obtained from Ref.[15] and the WZ parameters were derived using the effective masses presented in Ref.[13]. Since the conduction band is a parabolic model, we did not present the calculations.

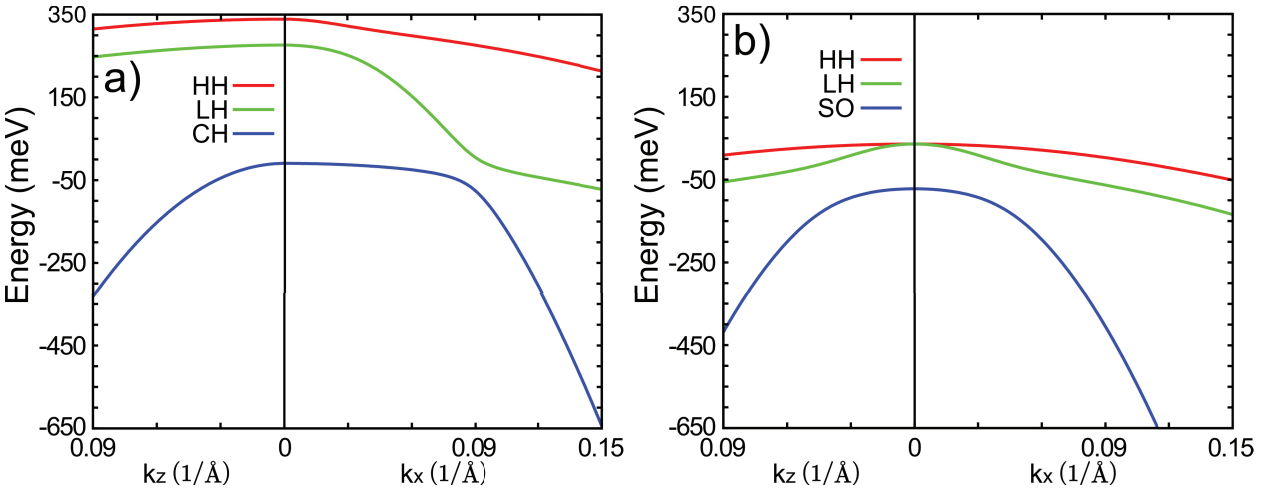

Figure 1: Valence band structure for bulk (a) WZ and (b) ZB. The usual identification of the bands was used for ZB while in WZ it was necessary to analyze the composition of the states in the Γ-point. We can see the anisotropy between k_z and k_x in WZ and also in ZB because in the new coordinate system the x and z axes do not reach equivalent points in the reciprocal space.

One can notice in figure 1 the explicit difference for both crystal structures. The WZ has three twofold degenerated bands in the Γ-point while ZB has one twofold degenerated and one fourfold degenerated. The anisotropy between the k_x and k_z direction can be noticed for WZ. This anisotropy also happens in ZB because the new axes do not reach equivalent points in the first Brillouin zone like in the [001] coordinate system.

As the typical dimensions of nanowhiskers are from 1 to several hundreds of Angstroms, in a first approximation we can neglect the effects of lateral confinement. Then a simple multiple quantum well (MQW) model can be used to simulate their band structures.

Using the envelope function approximation and considering different Bloch functions in each side of the interface as stated in equation (5), the parameters vary with the growth direction, making it possible to use a common matrix for both structures.

$$\psi(\vec{r}) = \sum_{l=1}^{8} e^{i(\vec{k}_\perp \cdot \vec{r}_\perp)} g_l(z) u_l^{WZ,ZB}(\vec{r}) \tag{5}$$

The z dependence in the growth direction of the parameters and envelope functions, $g_l(z)$, are treated with the

plane wave expansion

$$U(z) = \sum_{K_z} U_{K_z} e^{iK_z z} \tag{6}$$

where U_{K_z} are the Fourier coefficients of the z dependent function. The Fourier expansion also changes k_z to $k_z + K_z$ in the k·p matrix.

The total Hamiltonian of our model for a nanowhisker is

$$H_T(\vec{k}) = H_{k\cdot p}(\vec{k}) + V_{MQW} \tag{7}$$

where $H_{k\cdot p}(\vec{k})$ is the k·p term and V_{MQW} is a term that describes the band mismatch profile for the MQW.

3. Results and Discussion

The band offset for InP at the interface was given by [13] and the band alignment at $\vec{k} = 0$ for the diagonalized Hamiltonian can be found in figure 2a. This energy profile is characteristic of a type-II structure.

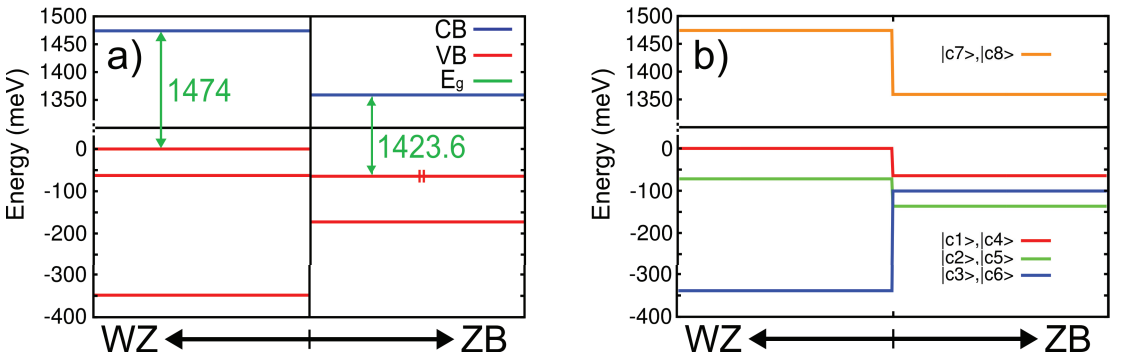

Figure 2: (a) The band edge energy in the WZ/ZB interface relating the WZ and ZB states. (b) The diagonal potential profile of the total Hamiltonian alongside the growth direction.

The diagonal terms of the total Hamiltonian at $\vec{k} = 0$ are presented in figure 2b. This is not the effective potential experienced by the carriers because the off diagonal term Δ couples the second (green) and third (blue) valence band states. Nevertheless, just looking to these energy diagrams it is easy to analyze the coupling of the different basis states across the barriers. So, using this point of view to this specific MQW profile one can expect having spatial carriers' separation.

Figure 3 displays the quantum well diagonal energy profile of the MQW system. We enumerate the conduction and valence band wells to identify the probability density of the carriers. Since 3 and 4 conduction wells have the same width, a degeneracy of states should be expected.

Figure 4 shows our calculations of the conduction and valence band structures up to 10% of the k_x direction and 100% of the k_z direction for the MQW system. All the states presented are inside the wells and the bands are nominated accordingly to the predominant basis state. The EL states are composed of $|c_7\rangle$ or $|c_8\rangle$, HH states are exclusively $|c_1\rangle$ or $|c_4\rangle$ and the LH states are a combination of $|c_2\rangle$ and $|c_6\rangle$ or $|c_5\rangle$ and $|c_3\rangle$, being $|c_2\rangle$ or $|c_5\rangle$ the major contribution. For the conduction band, The EL3 and EL4 states are nearly degenerate as it was expected since we have two wells of the same width. This effect is not seen in the valence band because all the wells have different widths.

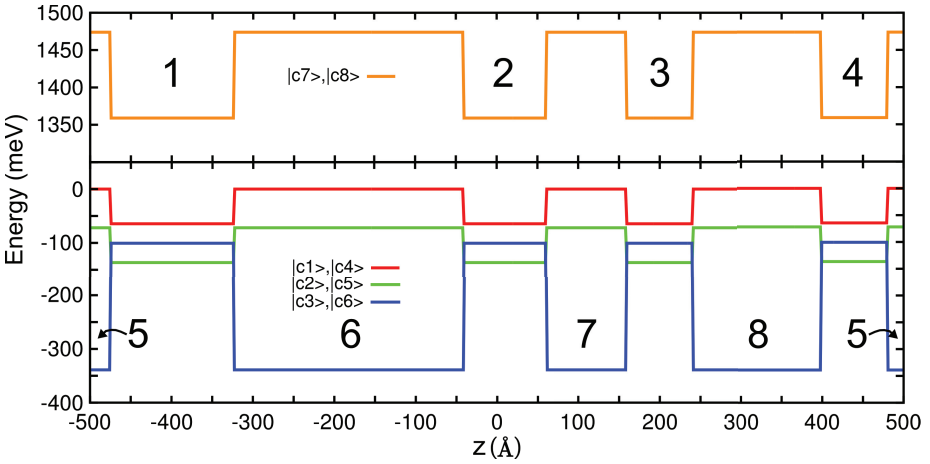

Figure 3: Diagonal terms of the total Hamiltonian at $\vec{k} = 0$ for the MQW system. The wells are numerated for identification purposes.

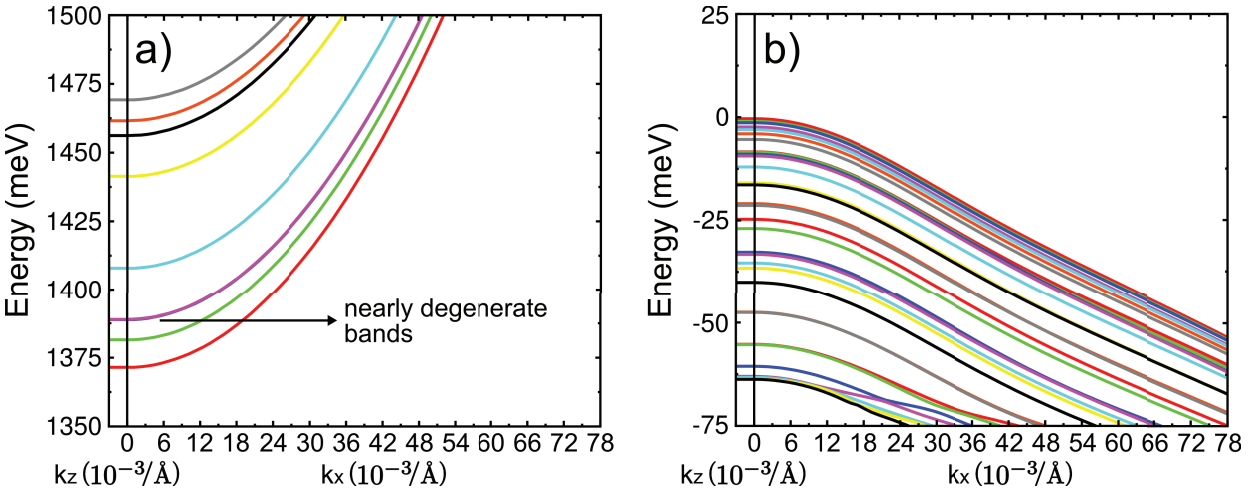

Figure 4: (a) Conduction band of the MQW structure. States from bottom to top: EL1 - EL9. The black arrow indicates the nearly degeneracy of EL3 and EL4 states. (b) Valence band of the MQW structure. States from top to bottom: HH1 - HH28, LH1, HH29 - HH30, LH2.

The dominant states, and their respective symmetry, play an important role in the luminescence spectra, for example, since the majority of the valence band states are HH the luminescence spectra is expected to be more intense perpendicularly to the growth direction. The contribution for luminescence spectra parallel to the growth direction comes from the LH states.

In figure 5 we show the probability densities calculated from the envelope functions and normalized in the reciprocal space at $\vec{k} = 0$ for EL1-EL4 and HH1-HH5 bands. The location of the states inside the wells of the MQW profile can be identified by the numbers in the figure and we can notice that the lower energy states belong to the larger wells. EL3 and EL4 are very similar because they belong to the wells of the same width in the conduction band. The narrowest well in the valence band, 5, begins to be occupied only by the HH9 state. As expected, the spatial separation of the carriers is observed: it is more likely to find holes in the WZ region and electrons in the ZB region, agreeing with experimental data.

Although we achieved reliable results with the model considered here, improvements should be made to treat other effects and also polytypism in other III-V compounds. To include higher bands, the basis rotation is no longer

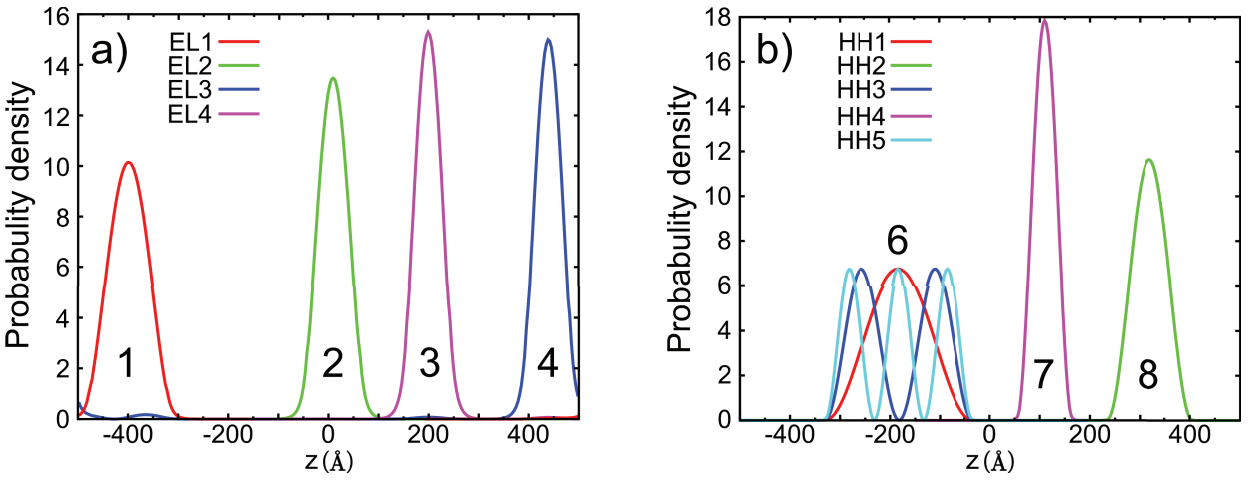

Figure 5: (a) Probability density of the conduction band states. (b) Probability density of the valence band states. We can notice the spatial separation of the carriers comparing the numbers to the MQW profile (figure 3).

useful, and a full symmetry analysis is necessary. We believe that this theoretical formulation based in the group theory concepts of the irreducible representations connection can lead to a better understanding and description of the polytypism effect in NWs.

4. Conclusion

We have presented a theoretical method relying on group theory arguments and the k·p method to calculate the electronic band structure of polytypical NWs in the vicinity of the Γ-point.

Our results for the MQW structure are in reasonable agreement with the experimental data available so far. We obtained the spatial separation of carriers and also light polarization trends in the luminescence spectra. According to our analysis of the valence band states composition, we expect the light emission to be more intense perpendicular to the growth direction.

It should be pointed out, however, that this is not a ultimate model and some improvements, such as the inclusion of strain, piezoelectric polarization and spontaneous polarization for WZ, are necessary in order to give a more accurate description of the polytypical NWs structures.

Acknowledgements

We like to thank the Brazilian funding agencies CAPES and CNPq for the financial support.

References

[1] J. Bao, D. C. Bell, F. Capasso, N. Erdman, D. Wei, L. Fröberg, T. Mårtensson, L. Samuelson, Advanced Materials 21 (2009) 3654–3658.
[2] J. Johansson, L. S. Karlsson, C. P. T. Svensson, T. Mårtensson, B. A. Wacaser, K. Deppert, L. Samuelson, W. Seifert, Journal of Crystal Growth 298 (2007) 635 – 639.
[3] J. Johansson, L. S. Karlsson, C. P. T. Svensson, T. Mårtensson, B. A. Wacaser, K. Deppert, L. Samuelson, W. Seifert, Nature Materials 5 (2005) 574–580.
[4] P. Caroff, K. A. Dick, J. Johansson, M. E. Messing, K. Deppert, L. Samuelson, Nature Nanotechnology 4 (2009) 50–55.
[5] M. Tchernycheva, G. E. Cirlin, G. Patriarche, L. Travers, V. Zwiller, U. Perinetti, J.-C. Harmand, Nano Letters 7 (2007) 1500–1504.
[6] Y. Kitauchi, Y. Kobayashi, K. Tomioka, S. Hara, K. Hiruma, T. Fukui, J. Motohisa, Nano Letters 10 (2010) 1699–1703.
[7] S.-G. Ihn, J.-I. Song, Y.-H. Kim, J. Y. Lee, I.-H. Ahn, Nanotechnology, IEEE Transactions on 6 (2007) 384 –389.
[8] V. Dubrovskii, G. Cirlin, V. Ustinov, Semiconductors 43 (2009) 1539–1584.
[9] E. G. Gadret, G. O. Dias, L. C. O. Dacal, M. M. de Lima Jr., C. V. R. S. Ruffo, F. Iikawa, M. J. S. P. Brasil, T. Chiaramonte, M. A. Cotta, L. H. G. Tizei, D. Ugarte, A. Cantarero, Physical Review B 82 (2010) 125327.

[10] D. Li, Z. Wang, F. Gao, Nanotechnology 21 (2010) 505709.
[11] M. Murayama, T. Nakayama, Phys. Rev. B 49 (1994) 4710–4724.
[12] P. E. Faria Junior, G. M. Sipahi, http://arxiv.org/abs/1012.0227.
[13] A. De, C. E. Pryor, Physical Review B 81 (2010) 155210.
[14] S. H. Park, S. L. Chuang, Journal of Applied Physics 87 (2000) 353.
[15] I. Vurgaftman, J. R. Meyer, L. R. Ram-Mohan, Journal of Applied Physics 89 (2001) 5815.